




タイトル Title	Visualization of intensive atrial inflammation and fibrosis after cryoballoon ablation: PET/MRI and LGE-MRI analysis
著者 Author(s)	Kiuchi, Kunihiro / Fukuzawa, Koji / Nogami, Munenobu / Watanabe, Yoshiaki / Takami, Mitsuru / Izawa, Yu / Negi, Noriyuki / Kyotani, Katsusuke / Mori, Shumpei / Hirata, Ken-Ichi
掲載誌・巻号・ページ Citation	Journal of Arrhythmia,37(1):52-59
刊行日 Issue date	2021-02
資源タイプ Resource Type	Journal Article / 学術雑誌論文
版区分 Resource Version	publisher
権利 Rights	© 2020 The Authors. Journal of Arrhythmia published by John Wiley & Sons Australia, Ltd on behalf of the Japanese Heart Rhythm Society. This is an open access article under the terms of the Creative Commons Attribution-NonCommercial License, which permits use, distribution and reproduction in any medium, provided the original work is properly cited and is not used for commercial purposes.
DOI	10.1002/joa3.12454
JaLDOI	
URL	http://www.lib.kobe-u.ac.jp/handle_kernel/90007883

Visualization of intensive atrial inflammation and fibrosis after cryoballoon ablation: PET/MRI and LGE-MRI analysis

Kunihiko Kiuchi MD¹  | Koji Fukuzawa MD¹ | Munenobu Nogami MD² | Yoshiaki Watanabe MD² | Mitsuru Takami MD¹ | Yu Izawa MD³ | Noriyuki Negi RT⁴ | Katsusuke Kyotani RT⁴ | Shumpei Mori MD³ | Ken-Ichi Hirata MD^{1,3}

¹Section of Arrhythmia, Division of Cardiovascular Medicine, Department of Internal Medicine, Kobe University Graduate School of Medicine, Kobe, Japan

²Department of Radiology, Kobe University Graduate School of Medicine, Kobe, Japan

³Division of Cardiovascular Medicine, Department of Internal Medicine, Kobe University Graduate School of Medicine, Kobe, Japan

⁴Division of Radiology, Center for Radiology and Radiation Oncology, Kobe University Hospital, Kobe city, Japan

Correspondence

Kunihiko Kiuchi, Division of Cardiovascular Medicine, Department of Internal Medicine, Kobe University Hospital, 7-5-2 Kusunoki-cho, Chuo-ku, Kobe city, Japan.
Email: kunihikiuchi@yahoo.co.jp

Funding information

This study is partly supported by JSPS KAKENHI Grant Number JP18K08036

Abstract

Background: Atrial inflammation plays an important role in initiating atrial fibrosis, which could perpetuate atrial fibrillation (AF). However, the method of visualization of atrial inflammation has not been established. We sought to investigate whether the intensive atrial inflammation caused by cryoballoon ablation (CBA) could be detected by positron emission tomography/ magnetic resonance imaging (PET/MRI) and whether the atrial inflammation could be associated with consequent fibrosis.

Methods: A total of 10 paroxysmal atrial fibrillation patients after CBA were enrolled. To detect and quantify intensive atrial inflammation, PET/MRI was performed to assess regional ¹⁸F-fluorodeoxyglucose (¹⁸F-FDG) uptake one day after the CBA, and the standardized uptake values (SUV) max were compared between the pulmonary vein (PV) antrum where CBA could be applied and the healthy left atrial (LA) wall where CBA could not be applied. Furthermore, the atrial inflammation one day after the procedure and atrial fibrosis areas one month after the procedure were three-dimensionally quantified by PET/MRI and late-gadolinium enhancement magnetic resonance imaging (LGE-MRI), respectively.

Results: The mean SUV max at the PV antrum was significantly higher than that on the healthy LA wall (2.12 ± 0.35 vs 1.73 ± 0.30 , $P = .00021$). The volume of the atrial inflammation strongly correlated with that of the atrial fibrosis ($r = .94$ [.76-.99], $P = .00006$).

Conclusions: The atrial inflammation after CBA could be detected by PET/MRI. CBA-induced atrial inflammation was strongly associated with consequent lesion maturation.

KEYWORDS

atrial fibrillation, cryoballoon, fibrosis, inflammation, PET/MRI

Abbreviations: ¹⁸F-FDG, ¹⁸F-fluorodeoxyglucose; AF, atrial fibrillation; CBA, cryoballoon ablation; CE-MRA, contrast enhancement-magnetic resonance angiography; CK, creatine kinase; CK-MB, creatine kinase MB; CRP, C-reactive protein; LGE-MRI, late-gadolinium enhancement magnetic resonance imaging; LIPV, left inferior pulmonary vein; LSPV, left superior pulmonary vein; PET/MRI, positron emission tomography/ magnetic resonance imaging; RIPV, right inferior pulmonary vein; RSPV, right superior pulmonary vein; SUV, standardized uptake value; TBR, target to background ratio.

This is an open access article under the terms of the Creative Commons Attribution-NonCommercial License, which permits use, distribution and reproduction in any medium, provided the original work is properly cited and is not used for commercial purposes.

© 2020 The Authors. *Journal of Arrhythmia* published by John Wiley & Sons Australia, Ltd on behalf of the Japanese Heart Rhythm Society.

1 | INTRODUCTION

Atrial remodeling involves electrophysiological and structural abnormalities that promote the development and perpetuation of atrial fibrillation (AF). Inflammation is reported to be associated with the initiation, perpetuation, and recurrence of AF.¹ Inflammatory biomarkers promote calcium handling abnormalities and provoke abnormal triggering and shortening of the atrial action potential duration. Atrial fibrosis is considered as an important factor perpetuating AF.² However, the mechanistic links between atrial fibrosis and inflammation are complex. Simultaneous positron emission tomography/magnetic resonance imaging (PET/MRI) was developed for functional and morphological imaging.³ PET/MRI has been used for visualization of the vessel wall inflammation and evaluation of the viability of the left ventricle, but has not been used for the visualization of "atrial" inflammation.⁴ Although atrial ¹⁸F-fluorodeoxyglucose (FDG) uptake in persistent AF patients has been reported from the whole-body PET/CT database as a retrospective study, no detailed distribution or quantitative analysis of atrial inflammation has been performed as a result of the thinner atrial wall and unstable cardiac rhythm and respiratory motion.⁵ Recently, we reported the feasibility of imaging inflammation in the left atrium (LA) after cryoballoon ablation (CBA) and hot balloon ablation as a pilot study.⁶ To extend diagnostic utility of the equipment (PET/MRI), we hereby conducted a prospective study to assess whether the atrial inflammation caused by CBA could be visualized using PET/MRI and whether it was associated with consequent fibrosis in AF patients.

2 | METHODS

2.1 | Study design

This study was an open-label, single-arm, prospective clinical trial and was registered with the University Hospital Medical Information Network-Clinical Trial Registry (UMIN-CTR) (UMIN000027417) and Japan Registry of Clinical Trials (jRCT) (jRCTs 052 180 024). The protocol for this study was approved by the local ethics committees of the institutions and conformed to the provisions of the Declaration of Helsinki (Committee of 17 August 2019, Approval No.C180014). The detailed protocol has been described previously.⁷ The primary endpoint was the visualization of the atrial inflammation by the PET/MRI. The secondary endpoint was atrial fibrosis following atrial inflammation.

2.2 | Study population

The patient inclusion criteria were as follows: (a) patients with AF who underwent CBA, (b) were aged 20-80 years, and (c) ability to provide written voluntary consent to participate in this study. After enrollment, PET/MRI and LGE-MRI were performed one day and one month after the CBA.

2.3 | Cryoballoon ablation procedure

The patients were studied under deep propofol sedation while breathing spontaneously. Unfractionated heparin was administered in a bolus form before the transseptal puncture to maintain an activated clotting time of >300 seconds.⁸

The mapping and ablation were performed using the NavX system (Abbott, Chicago, IL). Complete occlusion was confirmed by injecting contrast medium. The pulmonary vein isolation (PVI) was performed with a second-generation cryoballoon (Arctic Front Advance, Medtronic, Minneapolis, MN) with a freeze cycle of 180 seconds. If PV potentials remained, the operator decided whether additional CB ablation or touch-up RF ablation should be applied. The procedural endpoint was considered to be an electrophysiologically proven bidirectional block of the PV-encircling ablation lines confirmed with a circular mapping catheter (Optima, Abbott, Chicago, IL).

2.4 | ¹⁸F-FDG PET/MR imaging

¹⁸F-FDG PET/MRI imaging was performed on a simultaneous PET/MR scanner (Signa PET/MR, GE Medical Systems, Waukesha, WI, USA). Subjects fasted for >18 hours before the infusion of 3.5 MBq/kg of ¹⁸F-FDG (0.9 mCi/kg). The administration of heparin (50 IU/kg) prior to the scanning was performed. The PET emission scan was initiated 60 minutes after the administration of the ¹⁸F-FDG and continued for 30 minutes with the simultaneous acquisition of the MRI. A noncontrast-enhanced MRI (2-point Dixon 3-dimensional volumetric interpolated fast spoiled gradient echo, LAVA-Flex) was scanned for an attenuation correction and anatomic coregistration (slice thickness 5.2 mm/ gap 2.6 mm). Additionally, MRI scans were used for assessing the anatomy of the LA and pulmonary veins, including 2D-cine- and 3D-fast imaging employing a steady-state acquisition (FIESTA) and 3D-spoiled gradient recalled acquisition in the steady-state (SPGR). All the PET and MRI scans were performed simultaneously under respiratory- and cardiac-gating by using a navigator-echo technique and vectorcardiogram. The PET reconstruction parameters were as follows: ordered subset expectation maximization method OSEM with time-of-flight TOF; matrix, 512 × 512; slice thickness, 2.8; field of view, 60 cm; iterations, 3; subsets 16, Gaussian filter width, 4mm. To correct for any background noise from the ¹⁸F-FDG in the blood pool, the PET was also reconstructed by the TOF-block sequential regularized expectation maximization (Q.Clear®) method with a β value of 200-300. A detail setting of the β value has been previously described.⁷

2.5 | Quantitative analysis of atrial inflammation

The images were analyzed using commercially available workstations (Advantage Workstation ver 4.7; GE Medical Systems, Waukesha, WI, USA and Ziostation ver. 2.4.2.3.; Ziosoft Inc, Tokyo, Japan). The ¹⁸F-FDG uptake was assessed on the left atrial wall. From each

region of interest (ROI), the standardized uptake values (SUVs) were measured. The SUV represents the ^{18}F -FDG activity adjusted for the ^{18}F -FDG dose, corrected for any decay, and divided by the body weight according to the following formula: $\text{SUV} = \text{tissue tracer activity (MBq/mL)} / \text{injected dose per patient body weight (MBq/kg)}$. In the active segment analysis, the degree of the SUVmax was categorized by color-coded scaling (blue: <1.2 , green: <1.6 , yellow: <1.8 , orange: <2.2 and red: ≥ 2.2), whereas noninflamed segments were excluded. A 3D reconstruction of the color-coded FDG uptake and volume-rendered LA and PV was fused semiautomatically on the workstation. The volume-rendered LA and PV image was generated from the LAVA-Flex sequence. The area of the LA and PVs was determined by a consensus reading performed by a cardiologist with years of experience and a cardiovascular radiologist [YW] with 10 years of experience (Figure 1A).

To assess the atrial inflammation caused by CBA, the SUV max was compared between the PV antrum where CBA was applied and the other LA wall where no CBA was applied and a local voltage was

measured as >0.5 mV during sinus rhythm (SR). Furthermore, the volume of the atrial inflammation was defined as the area where the SUV max was greater than that on the normal voltage LA wall. In case when diffuse preexisting inflammation was found, we differentiate preexisting inflammation and inflammation post CBA based on the following: (a) whether the shape is artificial and continuous, (b) the distribution is consistent with that of scar area post CBA assessed by voltage map, (c) the degree of SUV max around PV and PV antrum is homogenous.

2.6 | LGE-MR imaging acquisition

All patients underwent contrast-enhanced MR imaging using a 1.5-T MR system (Achiva, Philips Medical, Best, The Netherlands) equipped with a 5-channel cardiac coil before and 1 month after the CBA. This scan technique has been established.^{9,10} First, contrast enhancement-magnetic resonance angiography (CE-MRA) of the PV-LA anatomy was acquired with a breath-hold 3D-fast field echo (FFE) sequence in the coronal plane during the first pass of a contrast agent (gadobutrol, Gadovist; Bayer Yakuhin, Osaka, Japan) injection at a dose of 0.1 mmol/kg. The LGE-MRI of the LA was to be acquired using a 3D inversion recovery, respiration navigated, electrocardiogram-gated, T1-FFE sequence in the transverse plane 15 minutes after the contrast injection, which has been previously reported.¹¹ The typical parameters were as follows: repetition time/echo time = 4.7/1.5 ms, voxel size = $1.43 \times 1.43 \times 2.40$ mm (reconstructed to $0.63 \times 0.63 \times 1.20$ mm), flip angle = 15, SENSE = 1.8, and 80 reference lines. The inversion time (TI) was set at 280–320 ms, using a Look-Locker scan. The data acquisition was performed during the mid-diastolic phase of the left ventricle. The typical scan time for the LGE-MRI study was 7–12 minutes depending on the patient's heart rate and respiration pattern. The images of the CE-MRA, and LGE-MRI were transferred to a workstation (Ziostation ver. 2.4.2.3., Ziosoft Inc, Tokyo, Japan) for further image postprocessing and an image analysis.

2.7 | Quantitative analysis of the atrial fibrosis

The following image postprocessing was performed by a consensus of a board-certified diagnostic radiologist and radiological technologist. The three-dimensional (3D) visualization method for the LGE was as follows.¹ An automatic adjustment of the CE-MRA and LGE-MRI using a positional reference as the table location was performed.² In the CE-MRA, a 3D image was segmented from the surrounding structures. The endocardial border of the LA wall (endo border) was determined by the anatomical information obtained from the 3D CE-MRA.³ We modified the CE-MRA with a 3 pixel enlarged volume automatically using the Workstation software. The possible epicardial border of the LA wall (possible epi border) was determined by the enlarged CE-MRA data.⁴ On the LGE-MRI, the LA wall segmentation was performed with the

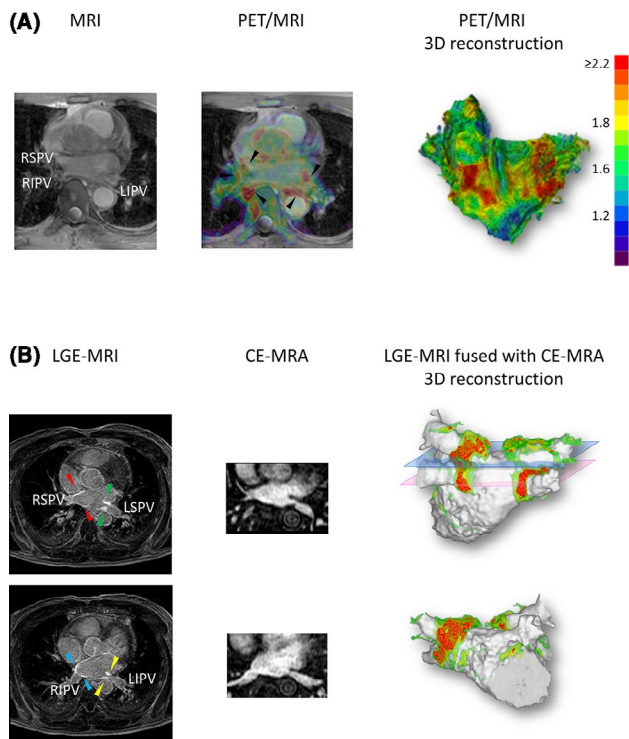


FIGURE 1 Visualization of atrial inflammation and fibrosis by PET/MRI and LGE-MRI. (A) PET/MRI, The black arrow indicates the intensive FDG uptake around the PV. (B) LGE-MRI (the left panel), CE-MRA (the middle panel), and 3D reconstruction of the LGE-MRI fused with CE-MRA (the right panel). The red and green arrows indicate the late-gadolinium enhancement of the RSPV and LSPV. The light blue and yellow arrows indicate that of the RIPV and LIPV. PET/MRI, positron emission tomography/magnetic resonance imaging; FDG, fluorodeoxyglucose; LGE-MRI, late-gadolinium enhancement magnetic resonance imaging; CE-MRA, contrast enhancement-magnetic resonance angiography; RSPV, right superior pulmonary vein; LSPV, left superior pulmonary vein; RIPV, right inferior pulmonary vein; LIPV, left inferior pulmonary vein

2-segmented MRA data including endo and possible epi borders.⁵ The LA wall on the LGE-MRI was segmented by subtracting from the possible epi border to endo border from the CE-MRA.⁶ The mean value and SD of the voxel intensity was measured on the “healthy” LA wall where no hyper-enhanced areas in the LGE-MRI were involved. A voxel intensity histogram analysis of the LA wall identified LGEs as intensities >2 SD on the “healthy” LA wall. Furthermore, the degree of the intensity was categorized by color-coded scaling (green: >2 SD; yellow: 3-4SD; and red: >4 SD). Finally, a 3D reconstruction of the color-coded LGE and volume-rendered LA and PV image generated from the CE-MRA were fused semiautomatically. In this study, to identify a more specific fibrotic region, atrial fibrosis after CBA was defined as an artificial LGE site with a signal intensity of >4 SD around the PV, and the volume was measured.⁹ To clarify the relationship between the atrial inflammation and fibrosis, the volume of the inflammation and that of the fibrosis were compared.

2.8 | Post interventional management and follow-up

If symptoms occurred outside the recording period, the patients were requested to contact our institution or the referring physician to obtain ECG documentation. AF episodes lasting longer than 30 seconds were considered recurrences.

2.9 | Statistical analysis

Continuous data were presented as mean \pm SD for normally distributed variables. Medians and quartiles were given for nonnormally distributed variables. If these data followed a normal distribution, they were tested with an unpaired *t*-test or Welch test. If not, they were tested with a Mann-Whitney test. Categorical variables were analyzed with the Fisher's exact test. Using a linear regression model, we evaluated the relationship between the atrial inflammation and following atrial fibrosis. A value of $P < .05$ was considered statistically significant. All statistical analyses were performed using SPSS, Release 24 software (SPSS, Chicago, IL, USA).

3 | RESULTS

3.1 | Patient and procedural characteristics

A consecutive 10 paroxysmal atrial fibrillation patients after the CBA were enrolled. The patient characteristics are shown in Table 1. The mean age was 54 ± 15 years old and nine patients were male. The mean left atrial diameter and left ventricular ejection fraction (LVEF) were 38 ± 6 mm and $62 \pm 9\%$, respectively. As for the procedural data, the CBA procedure time and fluoroscopy time were 167 ± 38 min and 46 ± 20 mm, respectively. Radiofrequency touch-up ablation for the RIPV was performed in one (10%) of 10 patients.

TABLE 1 Patient and procedural characteristics

	N = 10
Age, y	54 ± 15
Male, n (%)	9 (90)
Paroxysmal AF, n (%)	10 (100)
CHADS ₂ score, point	1 (0, 1)
LAA flow, cm/s	60 ± 20
LAD, mm	38 ± 6
LVEF, %	62 ± 9
BMI, kg/m ²	25 ± 5
BNP, pg/mL	97 ± 136
eGFR, ml/min/1.73 m ²	74 ± 15
CBA procedure time, min	167 ± 38
CBA fluoroscopy time, min	46 ± 20
Ablation duration of the LSPV, s	180 (180, 180)
Ablation duration of the LIPV, s	180 (180, 190)
Ablation duration of the RSPV, s	180 (180, 180)
Ablation duration of the RIPV, s	180 (180, 253)
RF touch-up ablation of the LSPV, n (%)	0 (0)
RF touch-up ablation of the LIPV, n (%)	0 (0)
RF touch-up ablation of the RSPV, n (%)	0 (0)
RF touch-up ablation of the RIPV, n (%)	1 (10)

Abbreviations: AF, atrial fibrillation; BMI, body mass index; BNP, brain natriuretic peptide; CBA, cryoballoon ablation; eGFR, estimated glomerular filtration rate; LAA, left atrial appendage; LAD, left atrial dimension; LIPV, left inferior pulmonary vein; LSPV, left superior pulmonary vein; LVEF, left ventricular ejection fraction; RF, radiofrequency; RIPV, right inferior pulmonary; RSPV, right superior pulmonary vein.

The cardiac rhythm was SR at the time of the PET/MRI and LGE-MRI acquisition in all patients.

3.2 | Visualization of the atrial inflammation and following atrial fibrosis

The mean SUV max at the PV antrum was significantly higher than that on the healthy LA wall (2.12 ± 0.35 vs 1.73 ± 0.30 , $P = .00021$). Individually, the SUV max at the PV antrum was also higher than on the LA wall in all patients (Figure 2A). The mean volume of the atrial inflammation and following fibrosis were 13.7 ± 11.0 cm³ and 2.9 ± 1.6 cm³, respectively. Of interest, the volume of the atrial inflammation was significantly associated with that of the atrial fibrosis ($r = .94$ [.76-.99], $P = .00006$) (Figure 2B). Figure 3 shows a representative case. Figure 3A shows case 7 with both intensive atrial inflammation and fibrosis and 3B, case 6 with both weak atrial fibrillation and fibrosis.

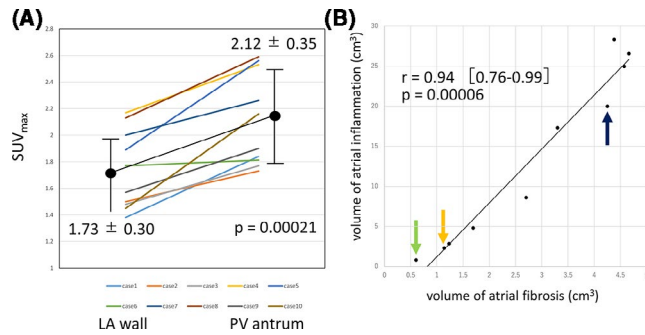


FIGURE 2 Quantitative analysis of atrial inflammation and fibrosis. (A) Comparison of the SUVmax between that at the PV antrum and on the healthy LA wall. The yellow, green, and dark blue indicate representative cases 4, 6, and 7, respectively. (B) Relationship between the volume of the atrial inflammation and that of atrial fibrosis. The yellow, green and dark blue arrows indicate representative cases 4, 6 and 7, respectively. The light green and yellow arrows indicate the patients with AF recurrence. SUV, standardized uptake value

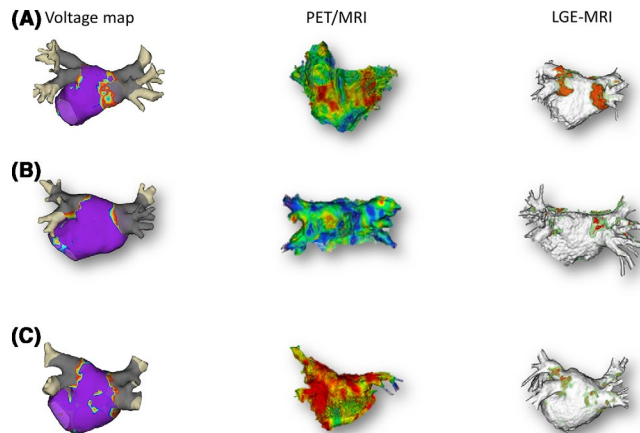


FIGURE 3 Representative cases. (A) Representative case 7 with a strong atrial inflammation and fibrosis volume. (B) Representative case 6 with a weak atrial inflammation and fibrosis volume. (C) Representative case 4 with both intensive induced and preexisting atrial inflammation but a weak fibrosis volume. The left panel shows the voltage map using the NavX system. The purple and gray indicate atrial voltages of >0.5 mV and <0.05 mV, respectively. An atrial voltage of 0.05 - 0.5 mV was colored. The middle panel shows the three-dimensionally reconstructed PET/MRI. The right panel shows the three-dimensionally reconstructed LGE-MRI. PET/MRI, positron emission tomography/ magnetic resonance imaging, LGE-MRI, late-gadolinium enhancement magnetic resonance imaging

3.3 | Biomarkers and atrial inflammation

C-reactive protein (CRP), creatine kinase (CK), and creatine kinase MB (CK-MB) were significantly increased after the CBA (CRP: 0.09 ± 0.11 to 0.84 ± 0.42 , $P = .0003$; CK: 201 ± 92 to 464 ± 154 , $P = .0002$; CK-MB: 5.9 ± 3.3 to 50.1 ± 27.5 , $P = .0005$). Although those values increased individually after the CBA, the degree varied

(Figure 4). The CRP level was not associated with the SUVmax at the PV antrum or atrial inflammation volume.

3.4 | Atrial inflammation and AF recurrence

AF recurred in two (29%) of seven patients during a median follow-up period of 12 [12, 12] months. Of note, the atrial inflammation volume and following atrial fibrosis were likely less in the two patients (cases 4 and 6) than in the others (atrial inflammation volume: 2.33 cm^3 in case 4 and 0.84 cm^3 in case 6; atrial fibrosis volume: 1.2 cm^3 in case 4 and 0.6 cm^3 in case 6). In the remaining five patients, the mean atrial inflammation and fibrosis volume were 15.5 ± 10 and $3.17 \pm 1.3 \text{ cm}^3$, respectively. In the 2nd procedure, no PV reconnection was found but distally isolated in case 4 and 4 PV reconnection was found in case 6. Non-PV foci were found at the LSPV antrum and LA posterior wall during ISP infusion in case 4. Therefore, Box lesion was performed. In case 6, PV reconnection was performed. No AF recurrence was found in both patients after the 2nd procedure. Figure 3C shows case 4 with AF recurrence in which intensive atrial inflammation was visible over the entire LA as well as around the PVs but the atrial fibrosis was likely less. In this case, the intensive inflammation was visible within PV, especially LSPV, LIPV and RSPV. This indicated the distal isolation. LGE-MRI demonstrated the LSPV stenosis one month after CBA. The other intensive inflammation was visible at the lateral LA and middle of the LA posterior wall where CBA was not applied, which was considered as the preexisting inflammation. Therefore, we considered that the inflammation post CBA was less which resulted in a small fibrosis area, but the PET-MRI showed a large inflammation as a result of the intensive preexisting inflammation.

4 | DISCUSSION

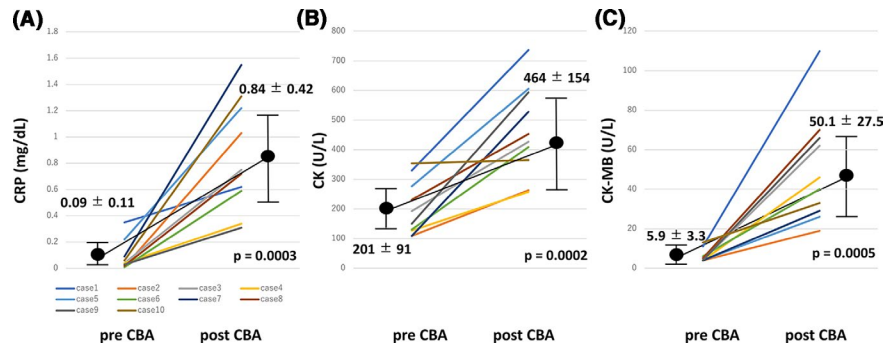
4.1 | Main findings

This study was the first to visualize the intensive atrial inflammation after CBA by using PET/MRI. The magnitude of the atrial inflammation could be associated with the consequent lesion maturation (fibrosis). To improve the imaging quality, the PET acquisition should be focused on the LA. A longer acquisition time (30minutes), completely controlled fast period of >18 hours, and heparin administration was necessary.

4.2 | Inflammatory response and cellular damage after CBA

Andrade reported that lesion formation with cryothermal ablation occurs through convective cooling. This process results in cold-induced cellular injury as a result of a combination of: (a) direct cellular damage secondary to an ice crystal formation and (b) ischemic

FIGURE 4 Biomarker analysis between pre- and post-CBA. Comparison of the CRP (A), CK (B), and CK-MB (C) between the pre- and post-CBA. CRP, C-reactive protein; CK, creatine kinase; CK-MB, creatine kinase MB



cell death as a result of microcirculatory failure.¹² The final phase of tissue injury consisted of reactive inflammation, followed by replacement fibrosis. These processes begin with thawing, and over several weeks culminate in the generation of a mature cryoablation lesion, which has a distinct, well-circumscribed central region of dense fibrosis surrounded by a narrow border zone of variable cellular death as a result of microvascular injury and apoptosis.¹³ Experimental data demonstrated that the intracellular ice formation could be induced immediately after cooling, which results in the cellular death.¹⁴ This direct tissue damage was determined by measurement of high-sensitive troponin T (hs-TnT) and procoagulant microparticles (MPs). Both biomarkers reached a peak 24 hours after the procedure and decreased thereafter. Subsequently, a significant inflammatory response as presented by an increase in hs-CRP was found. There was a trend toward a higher peak value between 24 to 48 hours after CBA.¹⁵ According to their results, the optimal timing of PET/MRI was considered as 24-48 hours after the CBA. Recently, Yano et al reported that inflammatory markers such as CRP is higher after RF ablation than after a CBA, whereas cellular damage markers such as a higher sensitive cardiac troponin I level are significantly higher after CBA. They speculated that the freeze and thaw process with cardiomyocyte swelling and membrane rupture might produce a greater elevation of myocardial injury markers but maintained the endothelial structure. However, radiofrequency energy could induce a relapse of endothelial inflammatory cytokines.¹⁶ We had previously reported the feasibility of imaging inflammation after both CBA and radiofrequency hot balloon ablation (RHA) as a case report, in which the FDG uptake was likely greater after RHA than after CBA.⁶ In this study, the CRP as well as creatine kinase (CK) and CK-MB increased significantly after the CBA. This finding indicated that CBA could induce atrial inflammation as well as atrial fibrosis, which was consistent with their results.

4.3 | Visualization of the atrial inflammation after CBA

Visualization of the atrial inflammation by PET/MRI is still challenging.¹⁷ Lange et al reported that routine 18F-FDG PET/CT could not detect inflammation in the LA in AF patients.¹⁸ Target to background ratios (TBR) were determined in the atrial and left ventricular walls and compared between the two groups. The TBR values of the LA

wall were not significantly higher in AF patients as compared to non-AF patients. As they speculated, the most critical limitation was that their study was designed in a retrospective fashion. Thus, patients were referred to the clinic for various indications such as malignancies and infections of unknown origin. Thus, the patients in this retrospective study did not fully represent the AF population. Another paroxysmal or chronic AF and non-AF were considered to be mixed. Furthermore, the limitation of that study was the lack of ECG data at the time of the scan. Cardiac rhythm such as AF further impaired the spatial resolution, increased image noise and reduced PET signal. Therefore, the low-level inflammation in the LA might not be adequately detected by PET. They strongly recommended that prospective clinical imaging studies in a larger homogeneous cohort of AF patients in the absence of systemic disease and relevant comorbidities using dedicated techniques for the suppression of the physiological myocardial glucose uptake such as a preparation with a “high fat low carb” diet and/or the administration of heparin prior to PET scanning should be considered.

In our study, most of the patients fasted for >18 hours. Fortunately, most of the patients fasted for >24 hours. The administration of heparin was carried out and SR was maintained in all patients. The magnitude of the atrial inflammation after the CBA might be greater than that of the preexisting original atrial inflammation. In fact, the mean SUVmax at the PV antrum of 2.10 in this study was greater than that on the LA wall of 1.21 in their study. Although the atrial wall was thin and influenced by cardiac and respiratory motion, we considered that the preparation could make it possible to adequately visualize the intensive atrial inflammation by PET/MRI.

4.4 | The magnitude of the atrial inflammation and following atrial fibrosis after CBA

Atrial fibrosis and edema after CBA could be visualized by LGE-MRI.¹⁹ The lesion maturation and durability could be assessed by LGE-MRI.²⁰ We previously reported that the lesion after CBA was characterized as a wide and continuous one.²¹ This indicated that CBA could induce intensive atrial fibrosis. Within hours of the CBA, a hemorrhagic state and inflammation occurred. At 6 weeks, the lesions were dense with collagen, fat deposition, and surrounded by a periphery of small blood vessels. After 12 weeks, the lesions were fibrotic and had no signs of inflammation. These findings were

obtained in animal models.¹³ In this study, we selected an earlier timepoint of MRI acquisition to avoid underestimating the ablation lesion because of the lesion shrinkage during the healing process and reverse remodeling. We hereby demonstrate that the magnitude of the inflammation after CBA could be strongly associated with that of fibrosis. The healing process after CBA such as from inflammation to fibrosis in the LA could be confirmed in humans.

4.5 | The magnitude of atrial inflammation and AF recurrence

Unlike the preexisting atrial inflammation, which was associated with systemic inflammatory disease and metabolic disorder, CBA-induced atrial inflammation was likely associated with ablation success.²² As compared to patients without AF recurrence, the CRP after the CBA, SUV max, and inflammation volume were much lower in the patients with AF recurrence. Of note, the lesions were much narrower, and many lesion gaps were documented in the AF recurrence patients. The CBA-induced intensive inflammation provided intensive fibrosis, which might be associated with the lesion durability. By focusing on AF recurrence, we speculated two mechanisms: (a) inadequate CBA-induced atrial inflammation and fibrosis, (b) progressed preexisting atrial inflammation and (c) both (a) and (b). By assessing the PET/MRI and LGE-MRI, the mechanism could be speculated. The mechanism of AF recurrence was considered as only (a) in case 6 but both (a) and (b) in case 4 (Figure 3B,C). Generally, patients with greater inflammatory response were reported to have early AF recurrence. This discrepancy might be caused by the distribution of the inflammation. In case when several CBAs was applied because of the difficulty of PVI, the balloon might be positioned more distally and the greater inflammation inside or near the PV ostium could induce the AF trigger from the PV antrum. In this study, we focused on the visible inflammation at the PV antrum. Therefore, the greater inflammation at the PV antrum might strongly eliminate AF trigger from the PV antrum.

4.6 | Low-grade atrial inflammation could be visible?

We were able to demonstrate that the atrial inflammation after CBA could be visualized by PET/MRI. However, the visualization of low-grade and preexisting atrial inflammation is still challenging. If an occlusion of the PV could be adequately obtained, the 3-minute CBA could provide a transmural lesion.²³ Such intensive atrial inflammation could be visualized by PET-MRI. In several retrospective studies, the imaging of the representative cases might have been special cases, because the SUVmax was similar to ours.¹⁷ This indicated that the magnitude of naturally occurring atrial inflammation was similar to that of artificially induced intensive atrial inflammation. In retrospective studies, such an intensive atrial inflammation might have been caused by other undetermined disorders. The important thing is whether low-grade atrial inflammation could be visualized by PET/MRI. To make it possible, further study is necessary.

4.7 | Study limitations

Our study had several limitations. First, the sample size was small. However, statistical significance could be achieved. Second, we performed no PET/MRI prior to the ablation procedure. Therefore, we could not discriminate between the CBA-induced atrial inflammation and preexisting atrial inflammation around the PVs. Third, touch-up RF ablation was performed. This might have influenced the magnitude of the atrial inflammation and following atrial fibrosis. Fourth, the timepoint of the LGE-MRI was 1 month after the CBA, which was earlier than in the previous studies. This indicated the possibility of overestimating the ablation lesion.

5 | CONCLUSION

Atrial inflammation after the CBA could be detected by PET/MRI during SR. The magnitude of the atrial inflammation one day after the CBA was strongly associated with the lesion maturation one month after the CBA. To improve the imaging quality, the importance was as follows: (a) an adequate fast time of >18 hours and the administration of heparin, (b) keeping SR during the PET/MRI, (c) a longer acquisition time of >30 minutes, and (d) adequate background noise reduction.

ACKNOWLEDGEMENTS

We would like to thank Mr John Martin for his linguistic assistance.

CONFLICTS OF INTEREST

The Section of Arrhythmia is supported by an endowment from Medtronic JAPAN and Abbott JAPAN. The authors have reported that they have no relationship relevant to the contents of this paper to disclose.

ORCID

Kunihiko Kiuchi  <https://orcid.org/0000-0002-9305-4854>

REFERENCES

1. Korantzopoulos P, Letsas KP, Tse G, Fragakis N, Goudis CA, Liu T. Inflammation and atrial fibrillation: a comprehensive review. *J Arrhythm*. 2018;34:394–401.
2. Kuo L, Zado E, Frankel D, Santangelli P, Arkles J, Han Y. Association of left atrial high-resolution late gadolinium enhancement on cardiac magnetic resonance with electrogram abnormalities beyond voltage in patients with atrial fibrillation. *Circ Arrhythm Electrophysiol*. 2020;13:e007586.
3. Judenhofer MS, Wehrl HF, Newport DF, Catana C, Siegel SB, Becker M. Simultaneous PET-MRI: a new approach for functional and morphological imaging. *Nat Med*. 2008;14:459–65.
4. van der Valk FM, Verweij SL, Zwinderman KA, Strang AC, Kaiser Y, Marquering HA. Thresholds for arterial wall inflammation quantified by 18F-FDG PET imaging: implications for vascular interventional studies. *JACC Cardiovasc Imaging*. 2016;9:1198–207.
5. Xie B, Chen BX, Wu JY, Liu X, Yang MF. Factors relevant to atrial (18)F-fluorodeoxyglucose uptake in atrial fibrillation. *J Nucl Cardiol*. 2018;27:1501–12.

6. Kiuchi K, Fukuzawa K, Mori S, Watanabe Y, Hirata KI. Feasibility of imaging inflammation in the left atrium post AF ablation using PET technology. *JACC Clin Electrophysiol*. 2017;3:1466–7.
7. Kiuchi K, Fukuzawa K, Nogami M, Watanabe Y, Takami M, Mori S. Visualization of inflammation after cryoballoon ablation in atrial fibrillation patients - protocol for proof-of-concept feasibility trial. *Circulation Rep*. 2019;1:149–52.
8. Kiuchi K, Kircher S, Watanabe N, Gaspar T, Rolf S, Arya A. Quantitative analysis of isolation area and rhythm outcome in patients with paroxysmal atrial fibrillation after circumferential pulmonary vein antrum isolation using the pace-and-ablate technique. *Circ Arrhythm Electrophysiol*. 2012;5:667–75.
9. Kiuchi K, Okajima K, Shimane A, Yokoi K, Teranishi J, Aoki K. Visualization of the radiofrequency lesion after pulmonary vein isolation using delayed enhancement magnetic resonance imaging fused with magnetic resonance angiography. *J Arrhythm*. 2015;31:152–8.
10. Kurose J, Kiuchi K, Fukuzawa K, Takami M, Mori S, Suehiro H. Lesion characteristics between cryoballoon ablation and radiofrequency ablation with a contact-force sensing catheter: late-gadolinium enhancement magnetic resonance imaging assessment. *J Cardiovasc Electrophysiol*. 2020 <https://doi.org/10.1111/jce.14664> in press
11. McGann C, Akoum N, Patel A, Kholmovski E, Revelo P, Damal K, et al. Atrial fibrillation ablation outcome is predicted by left atrial remodeling on MRI. *Circ Arrhythm Electrophysiol*. 2014;7:23–30.
12. Andrade JG, Khairy P, Dubuc M. Catheter cryoablation: biology and clinical uses. *Circ Arrhythm Electrophysiol*. 2013;6:218–27.
13. Avitall B, Kalinski A. Cryotherapy of cardiac arrhythmia: from basic science to the bedside. *Heart Rhythm*. 2015;12:2195–203.
14. Gao D, Critser JK. Mechanisms of cryoinjury in living cells. *Ilar J*. 2000;41:187–96.
15. Herrera Siklódy C, Arentz T, Minners J, Jesel L, Stratz C, Valina CM, et al. Cellular damage, platelet activation, and inflammatory response after pulmonary vein isolation: a randomized study comparing radiofrequency ablation with cryoablation. *Heart Rhythm*. 2012;9:189–96.
16. Yano M, Egami Y, Yanagawa K, Nakamura H, Matsuhira Y, Yasumoto K, et al. Comparison of myocardial injury and inflammation after pulmonary vein isolation for paroxysmal atrial fibrillation between radiofrequency catheter ablation and cryoballoon ablation. *J Cardiovasc Electrophysiol*. 2020;31:1315–22.
17. Watanabe E, Miyagawa M, Uetani T, Kinoshita M, Kitazawa R, Kurata M, et al. Positron emission tomography/computed tomography detection of increased (18)F-fluorodeoxyglucose uptake in the cardiac atria of patients with atrial fibrillation. *Int J Cardiol*. 2019;283:171–7.
18. Lange PS, Avramovic N, Frommeyer G, Wasmer K, Pott C, Eckardt L, et al. Routine (18)F-FDG PET/CT does not detect inflammation in the left atrium in patients with atrial fibrillation. *Int J Cardiovasc Imaging*. 2017;33:1271–6.
19. Cochet H, Dubois R, Yamashita S, Jefairi NA, Berte B, Sellal JM. Relationship between fibrosis detected on late gadolinium-enhanced cardiac magnetic resonance and re-entrant activity assessed with electrocardiographic imaging in human persistent atrial fibrillation. *JACC Clin Electrophysiol*. 2018;4:17–29.
20. Akita T, Kiuchi K, Fukuzawa K, Shimane A, Matsuyama S, Takami M, et al. Lesion distribution after cryoballoon ablation and hotballoon ablation: late-gadolinium enhancement magnetic resonance imaging analysis. *J Cardiovasc Electrophysiol*. 2019;30:1830–40.
21. Kurose J, Kiuchi K, Fukuzawa K, Mori S, Ichibori H, Konishi H. The lesion characteristics assessed by LGE-MRI after the cryoballoon ablation and conventional radiofrequency ablation. *J Arrhythm*. 2018;34:158–66.
22. Packer M. Characterization, pathogenesis, and clinical implications of inflammation-related atrial myopathy as an important cause of atrial fibrillation. *J Am Heart Assoc*. 2020;9:e015343.
23. Takami M, Lehmann HI, Misiri J, Parker KD, Sarmiento RI, Johnson SB, et al. Impact of freezing time and balloon size on the thermodynamics and isolation efficacy during pulmonary vein isolation using the second generation cryoballoon. *Circ Arrhythm Electrophysiol*. 2015;8:836–45.

How to cite this article: Kiuchi K, Fukuzawa K, Nogami M, et al. Visualization of intensive atrial inflammation and fibrosis after cryoballoon ablation: PET/MRI and LGE-MRI analysis. *J Arrhythmia*. 2021;37:52–59. <https://doi.org/10.1002/joa3.12454>